Phosphorene: Synthesis, Scale-Up, and Quantitative Optical Spectroscopy

Adam H. Woomer,[†,⊥] Tyler W. Farnsworth,[†,⊥] Jun Hu,[†] Rebekah A. Wells,[†] Carrie L. Donley,[‡] and Scott C. Warren[*,†,§]

[†]Department of Chemistry, [‡]Chapel Hill Analytical and Nanofabrication Laboratory, and [§]Department of Applied Physical Sciences, University of North Carolina at Chapel Hill, Chapel Hill, North Carolina 27599, United States. [⊥]A.H.W. and T.W.F. contributed equally.

ABSTRACT Phosphorene, a two-dimensional (2D) monolayer of black phosphorus, has attracted considerable theoretical interest, although the experimental realization of monolayer, bilayer, and few-layer flakes has been a significant challenge. Here, we systematically survey conditions for liquid exfoliation to achieve the first large-scale production of monolayer, bilayer, and few-layer phosphorus, with exfoliation demonstrated at the 10 g scale. We describe a rapid approach for quantifying the thickness of 2D phosphorus and show that monolayer and few-layer flakes produced by our approach are crystalline and unoxidized, while air exposure leads to rapid oxidation and the production of acid. With large quantities of 2D phosphorus now available, we perform the first quantitative measurements of the material's absorption edge—which is nearly identical to the material's band gap under our experimental conditions—as a function of flake thickness. Our interpretation of the absorbance spectrum relies on an analytical method introduced in this work, allowing the accurate determination of the absorption edge in polydisperse samples of quantum-confined semiconductors. Using this method, we found that the band gap of black phosphorus increased from 0.33 ± 0.02 eV in bulk to 1.88 ± 0.24 eV in bilayers, a range that is larger than that of any other 2D material. In addition, we quantified a higher-energy optical transition (VB−1 to CB), which changes from 2.0 eV in bulk to 3.23 eV in bilayers. This work describes several methods for producing and analyzing 2D phosphorus while also yielding a class of 2D materials with unprecedented optoelectronic properties.

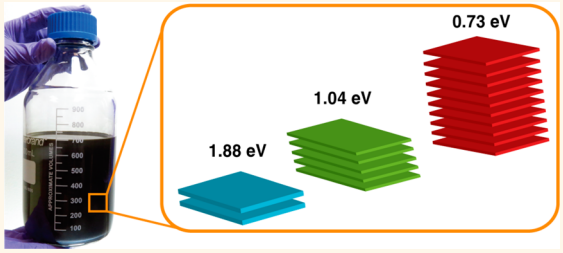

KEYWORDS: phosphorene · black phosphorus · liquid exfoliation · band gap · quantum confinement · 2D materials · optical spectroscopy

Solution-processable nanomaterials with tunable optoelectronic properties are being considered as potential building blocks for numerous technologies, such as photovoltaics,[1] transistors,[2] and light-emitting diodes.[3] Among these nanomaterials, quantum dots have attracted broad interest because of their size-dependent electronic structure and controllable physical properties; for example, band gaps can be increased by as much as 2 eV as particle size decreases.[4−7] With the advent of two-dimensional (2D) semiconductors,[8] new opportunities have emerged for designing materials and devices, although the size-dependent variation of electronic properties like band gaps are, in general, smaller: transition metal dichalcogenides have band gaps that can only be tuned by 0.7 eV,[9,10] while, for example, PbSe quantum dots can be tuned from 0.27 to 1.5 eV.[11−13] Toward increasing the library of solution-processable materials, we show here that black phosphorus can be liquid exfoliated to yield a family of 2D flakes with tunable optical properties that rival those of quantum dots.

Black phosphorus,[14] a layered 3D crystal of elemental phosphorus (Figure 1a), and its 2D derivative, termed phosphorene[15,16] (Figure 1b), have recently attracted renewed[17] attention. In the last few months, there have been exciting demonstrations of the material's application to transistors,[16,18,19] photovoltaics,[20,21] photodetectors,[22,23] and batteries.[24,25] As a 2D material with an intriguing corrugated or accordion-like structure, phosphorene has captured significant theoretical interest with numerous predictions of the material's anisotropic[16,26] and thickness-dependent optoelectronic properties,[27,28] mechanical properties,[29] and chemical reactivity.[30−32] Most predictions have gone untested, however, because there is still no reliable method to make or purify monolayer or few-layer

* Address correspondence to sw@unc.edu.

Received for review April 28, 2015 and accepted August 9, 2015.

Published online August 09, 2015
10.1021/acsnano.5b02599

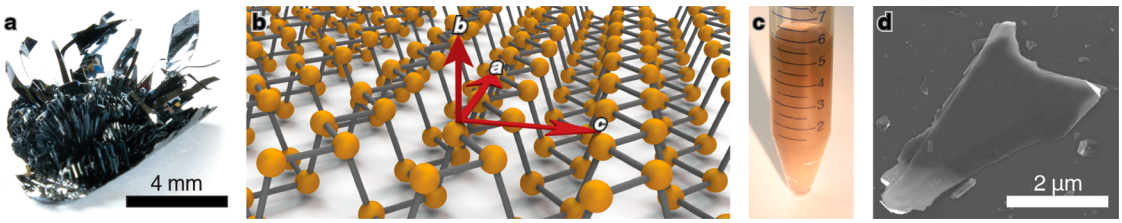

Figure 1. Liquid exfoliation of black phosphorus. (a) Photograph of black phosphorus grown by chemical vapor transport. (b) Illustration of a phosphorene monolayer showing the conventional crystallographic axes. The zigzag direction is "a", the armchair direction is "c", and the "b" direction is normal to the flake. (c) Photograph of a liquid-exfoliated suspension of 2D phosphorus in isopropyl alcohol. (d) SEM image of liquid-exfoliated 2D phosphorus.

phosphorus. When monolayers have been observed, they are typically situated at the edges of thicker sheets and are typically too small to characterize. Underlying these practical challenges are the inherent problems associated with phosphorus: the phosphorus–phosphorus bonds are significantly weaker than carbon–carbon bonds, and several studies have noted the material's tendency to oxidize[14,33] or form other allotropes.[34,35] In addition, interlayer interactions may be stronger in black phosphorus than in other 2D materials.[36,37] These strong interlayer interactions would inhibit exfoliation, and consequently, black phosphorus may be harder to exfoliate and more likely to fragment than other 2D materials. In fact, this is consistent with reports of mechanical exfoliation in which sheets of fewer than six layers have seldom been observed.[16,18,19,38,39]

Our own attempts to mechanically exfoliate black phosphorus confirmed the results of other groups. We prepared and analyzed samples under an inert atmosphere, using scotch tape for exfoliation and a Bruker Dimension FastScan atomic force microscope (AFM) to rapidly analyze sheet thickness over macroscopic areas (see Supporting Information for additional details). We randomly surveyed large areas and assessed the structure of over 3000 flakes. Our survey revealed that the yield of sheets thinner than 10 layers is less than 0.06%; in addition, no sheets thinner than six layers were found. Given the low odds for identifying and characterizing 2D materials prepared in this way, we began exploring liquid exfoliation[40,41] as an alternative route for material preparation. Here, we provide evidence that liquid exfoliation, when carefully executed under an inert atmosphere, produces macroscopic (milligram-to-gram scale) quantities of monolayer and few-layer phosphorene.[42] We note that this is a considerable improvement over state-of-the-art methods of liquid exfoliation,[43–45] which have so far produced flakes with thicknesses that are 10–20 times thicker than those described here. We characterize the material's structure, stability, and thickness-dependent optical properties and compare these properties to theoretical predictions. In addition, we perform the first quantitative optical absorption measurements on 2D phosphorus, allowing us to determine the thickness-dependent optical transitions and band gaps.

RESULTS AND DISCUSSION

Liquid Exfoliation of Black Phosphorus. Black phosphorus crystals (Figure 1a) were acquired from Smart Elements between December 2012 and March 2014 or were grown in our laboratory by SnI_2 vapor transport.[46] (Smart Elements modified its method of manufacture in the summer of 2014, and the microstructures of materials acquired after this date may differ.) Black phosphorus was ground in a mortar and pestle and sonicated in anhydrous, deoxygenated organic liquids using low-power bath sonication under an inert atmosphere. In our initial experiments, black phosphorus was sonicated in electronic grade isopropyl alcohol (IPA) for 16 h. During sonication, the phosphorus was suspended in solution and its color changed from black to reddish-brown (Figure 1c), indicating a profound change in the electronic structure of the material. We quantified this change in appearance by ultraviolet–visible–near-infrared (UV–vis–NIR) absorption spectroscopy (see discussion below for further details). Over several weeks, there was limited reaggregation and no further change in color, suggesting that these suspensions comprised small phosphorus particulates. To examine the morphology of the particulates, suspensions were drop-cast onto a silicon wafer for analysis by scanning electron microscopy (SEM, Figure 1d). These images confirmed the presence of thin phosphorus flakes with lateral dimensions between 50 nm and 50 μm. From these results, we concluded that a more extensive study was required to identify conditions that maximized the yield of thin phosphorus flakes.

We surveyed[42] 18 solvents for their ability to exfoliate black phosphorus (see Supporting Information for full experimental details). Black phosphorus (10 mg) was added to 20 mL of each solvent and sonicated for 13 h under anhydrous and air-free conditions. The suspensions were centrifuged at 3000*g* for 30 min to remove unexfoliated black phosphorus. The supernatant was further purified *via* dialysis to remove small (<2.5 nm) phosphorus fragments. These suspensions were characterized with inductively coupled plasma

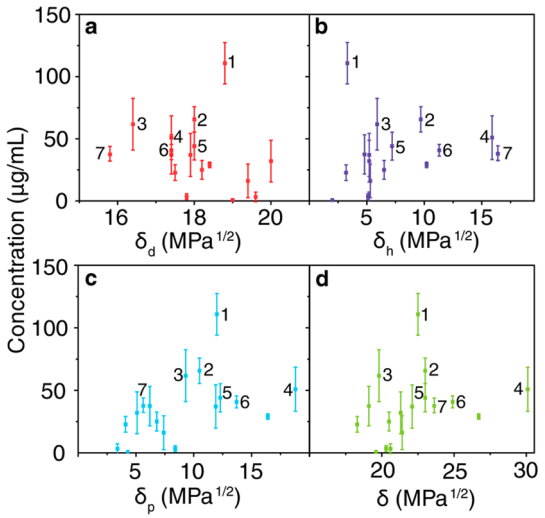

Figure 2. Survey of organic liquids, showing 2D phosphorus concentrations *vs* Hansen (a−c) and Hildebrand (d) solubility parameters for 18 solvents. The Hansen plots depict the energy due to dispersion forces (a), hydrogen bonding (b), and dipolar intermolecular forces (c). Numbers 1 through 7 rank the best liquids: (1) benzonitrile, (2) 1,3-dimethyl-2-imidazolidinone, (3) 1-vinyl-2-pyrrolidinone, (4) *N*-methylformamide, (5) *N*-methyl-2-pyrrolidone, (6) *N*, *N*-dimethylformamide, (7) 2-propanol. Each data point is an average of three trials; the error bars correspond to the standard deviation.

mass spectroscopy (ICP-MS) and UV−vis transmission spectroscopy to measure a dispersed concentration. We found that the best solvent was benzonitrile, which achieved a mean concentration of 0.11 ± 0.02 mg/mL. Plots of phosphorus concentration *versus* the Hansen solubility parameters of each solvent (Figure 2a−d) allow us to estimate that the Hildebrand parameter for 2D phosphorus is 22 ± 3 $MPa^{1/2}$. Although there is significant solvent-to-solvent variability—a feature common to graphene, boron nitride, and transition metal dichalcogenides[41]—we find that the optimal solvents for 2D phosphorus are similar to those for other 2D materials. An essential difference, however, is that 2D phosphorus must be handled and sonicated under an inert atmosphere, as we demonstrate below.

Characterization of 2D Phosphorus. In order to examine the structure of the suspended material, we used transmission electron microscopy (TEM) to quantify shape, size, and thickness as well as high-resolution TEM (HR-TEM) to assess crystallinity. We imaged and measured thousands of phosphorus flakes; Figure 3a−c shows TEM images of several representative samples. As before, a broad distribution of flake sizes was found. Single pieces typically had uniform contrast, suggesting that they had a planar morphology. All of the pieces examined in HR-TEM exhibited lattice fringes, showing that the crystallinity of phosphorus flakes was preserved (Figure 3d). We analyzed HR-TEM images by performing fast Fourier transforms (FFT), allowing us to observe the expected {200} and {002} plane families of black phosphorus. In addition, some flakes exhibited strong 101 intensities (Figure 3e), which are forbidden sets of diffracting planes in bulk black phosphorus. To understand the origin of the 101 spots, we used multislice calculations (JEMS[47]) to simulate HR-TEM images of 2D phosphorus sheets with varying thicknesses from four common microscopes (see Supporting Information for additional details). Fast Fourier transforms were applied to the HR-TEM images to determine the intensities of spots corresponding to plane families. In agreement with a previous analysis of electron diffraction patterns,[28] we found that a large 101:200 intensity ratio in FFTs is a unique characteristic of monolayers (Figure 3f) when imaged at or near Scherzer defocus, thus confirming their presence in our suspensions. We attribute the diffuse background of the FFT (Figure 3e) to the likely presence of absorbed organics, which has been observed previously for other 2D materials that were not degassed at elevated temperatures prior to imaging.[48,49]

To quantify the thickness of all flakes in our suspensions, we used our real-space TEM images—all acquired under identical imaging conditions including exposure time, aperture selection, lens currents, magnification, and defocus value—to measure the change in intensity across sheet edges for hundreds of flakes (Figure 3a, line and inset). Flake edges were suspended over either vacuum or carbon film (see Supporting Information for additional details). The smallest intensity change was 25 ± 3 counts, and all other intensity changes were multiples of 25 counts (Figure 3c, inset). We therefore assigned an intensity change of 25, 50, 75, and 100 counts to monolayers, bilayers, trilayers, and four-layered 2D phosphorus flakes, respectively. Further confirming this assignment, we found that only those flakes with a contrast change of *ca.* 25 counts had the intense 101 spots that are a hallmark of monolayers. Although this method is simple and fast, we do note that the linear relationship breaks down for flakes that are thicker than *ca.* 40 layers.

With the goal of isolating 2D flakes with well-defined thicknesses and optical properties, we used centrifugation to fractionate the phosphorus suspensions. We centrifuged the mixture at a rotational centrifugal force (rcf) as low as 120*g* and then centrifuged the supernatant at a slightly greater rcf, reaching values of up to 48 000*g*. The sediment from the second centrifugation was collected and redispersed in pure solvent. This new suspension is labeled by the average centrifugal force between the two rcf values; for example, a suspension labeled 20 200*g* has been centrifuged at 17 200*g* and 23 400*g* (see Supporting Information for full experimental details). Using TEM, we analyzed the thicknesses (Figure 4a) and lateral sizes (Figure 4b) of the suspended 2D phosphorus flakes. We found that this centrifugation approach could systematically isolate flakes with varying size and thickness distributions. When high centrifugation

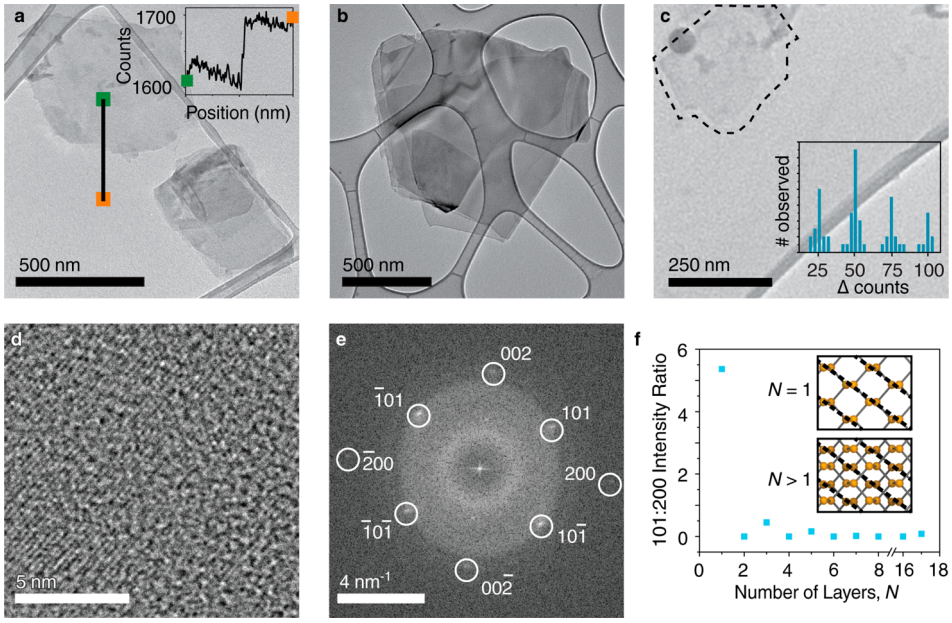

Figure 3. TEM characterization of liquid-exfoliated 2D phosphorus. (a–c) TEM images of 2D phosphorus. (c) TEM image of a monolayer of 2D phosphorus. The inset in (a) shows the contrast change (*ca.* 75 counts) from a line profile drawn across a flake that is three layers thick. The inset in (c) provides a histogram of contrast changes from 100 flakes. The changes in intensity (25, 50, *etc.*) correspond to monolayers, bilayers, *etc.* (d) HR-TEM image of phosphorene, a monolayer. (e) FFT of the HR-TEM image in (d). (f) Intensity ratios of 101 and 200 spots in FFT HR-TEM images and their relation to layer thickness, as calculated from multislice simulations in JEMS.[47] Insets show that constructive interference from {101} plane families (dashed lines) occurs in monolayers but has low or no intensity in multilayer flakes.

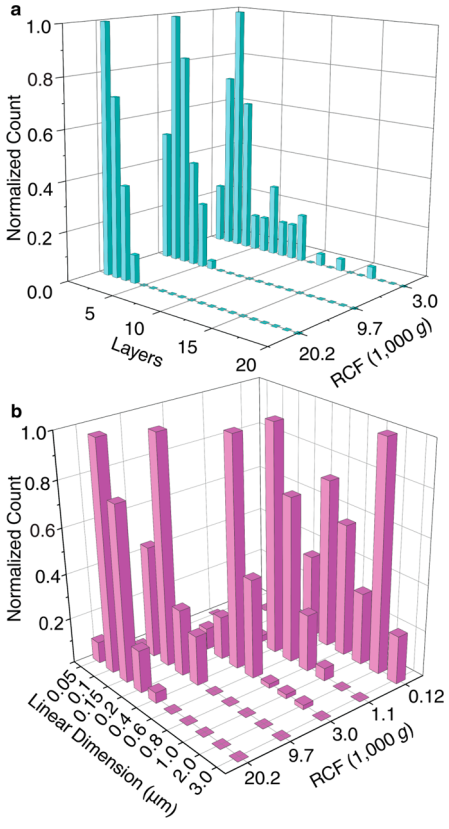

Figure 4. Selective variation of the centrifugation rate allows for control over flake thickness (a) and flake lateral size (b).

speeds were used, for example, we collected macroscopic quantities of flakes with size distributions centered near one-layer and two-layer thicknesses (Figure 4a), in which monolayers comprised up to 45% of the sample. Phosphorene—a material that has been sought after but rarely observed—is now easily accessible.

Stability of Phosphorene and 2D Phosphorus. As first recognized by Bridgman[14] in 1914, black phosphorus oxidizes and converts to phosphoric acid under humid atmospheric conditions. More recent studies have also shown that mechanically exfoliated phosphorus degrades in air.[19,28,32] We used X-ray photoelectron spectroscopy (XPS) and measurements of apparent pH to assess the oxidation. We performed XPS both on bulk black phosphorus to obtain a reference spectrum (Figure 5a) and on 2D phosphorus to test whether oxidation accompanies liquid exfoliation (Figure 5b). In addition to performing all exfoliation and centrifugation under an inert atmosphere, we constructed a transfer chamber that excluded oxygen and water during sample transfer to and from the XPS instrument (see Supporting Information for experimental details). Pristine black phosphorus had $2p_{1/2}$ and $2p_{3/2}$ peaks that are characteristic of unoxidized elemental phosphorus.[50] We exposed the same sample to air and reacquired XPS spectra at later time intervals. A broad peak at 134 eV emerged, which can be attributed to several types of phosphorus–oxygen bonds.[51] Without an oxidation mechanism, we cannot yet identify the type or types of P–O species that may be present in our samples. We performed similar experiments on

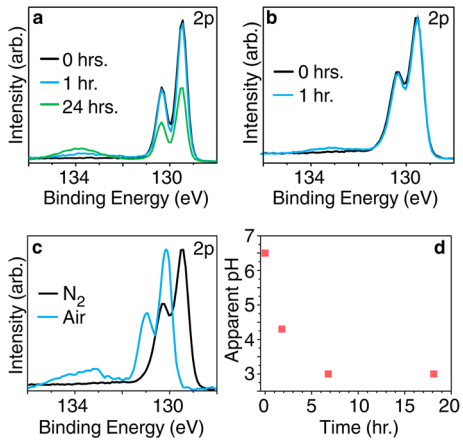

Figure 5. (a) XPS of freshly cleaved bulk black phosphorus after exposure to ambient air and room light for 0 (black), 1 (blue), and 24 h (green). (b) XPS analysis of few-layer 2D phosphorus showing that the material prepared by liquid exfoliation was unoxidized (black). The few-layer sheets were controllably oxidized by exposure to light (λ = 460 nm) and oxygen with some water (blue). (c) Exfoliation of black phosphorus in a sealed vial with N_2 (black) or air (blue) in the head space of the vial shows that the presence of air causes 28% of the phosphorus to become oxidized. Binding energies also increase, although the origin of this effect—whether sample charging, doping, or both—is not yet clear. (d) When few-layer 2D phosphorus (<6 layers) is suspended in isopropyl alcohol and exposed to light and air (λ = 460 nm), the apparent pH (recorded by a pH meter) decreases because of acid production.

thin 2D phosphorus (<6 layers). The pristine sample exhibited no signs of oxidation (Figure 5b, black). Upon exposure to oxygen gas that contained some water (not dried) and 460 nm light, a broad peak appeared at 133 eV, characteristic of oxidized phosphorus. In this modified material, *ca.* 5% of the phosphorus was oxidized, as estimated by peak integration software. Collectively, our analyses demonstrate that liquid exfoliation successfully yields high-quality, unoxidized 2D phosphorus.

In order to evaluate whether handling under an inert atmosphere is important, we sonicated black phosphorus in a sealed vial, with either nitrogen or air in the vial's head space. Analysis of the air-exposed material by XPS (Figure 5c) shows substantial oxidation, with 28% of the phosphorus no longer in the unoxidized form. In addition, we monitored the pH of a solution of few-layer phosphorus that was suspended in isopropyl alcohol and exposed to light and air (Figure 5d). We found that the solution rapidly acidifies, consistent with Bridgman's prediction[14] that phosphoric acid is produced upon exposure to air. When higher phosphorus concentrations are used, the apparent change in pH is larger. On the basis of these and prior findings,[43] we conclude that although liquid exfoliation in the presence of air may produce some crystalline, thin material, its surfaces and interior[52] are oxidized, acid is present, and its overall quality is low.

Exfoliation of Black Phosphorus at the 10 g Scale. We explored shear mixing[42,53] as a method for the scaled-up production of 2D phosphorus. We used a Silverson L5M-A shear mixer with either a 0.75 or 1.385 in. rotor with square holes for our work at the 1 and 10 g scales, respectively. All experiments were performed under oxygen-free and water-free conditions by bubbling nitrogen gas into the mixing container. In addition, we used a water bath to keep the solutions at room temperature during mixing. We used several different grades of *N*-methyl-2-pyrrolidone (NMP), as it was disclosed to us by the Coleman group that only certain types of NMP may work for shear mixing of graphene.[54] Ultimately, we selected NMP from Sigma-Aldrich (99.5% purity, anhydrous) for our scaled-up exfoliation. Black phosphorus was ground in a mortar and pestle prior to its use in shear mixing. We used two different grades of black phosphorus, both of which we produced in our laboratory. The first "high-quality" black phosphorus was highly crystalline with millimeter-sized crystals and was difficult to grind; the second "low-quality" black phosphorus was highly polycrystalline, had trace amounts of red phosphorus, and was easy to grind. In our experiments, we found that only the low-quality material could be successfully exfoliated by shear mixing alone, regardless of the type of NMP or the conditions of shear mixing. This observation is consistent with a mechanism in which the separation of layers is nucleated at grain boundaries or other defects in the material. In order to exfoliate the higher-quality starting material, we had to rely on a combination of shear mixing and bath sonication.

For our scaled-up synthesis, we dispersed 6 g of pulverized, high-quality black phosphorus into 100 mL of NMP and bath sonicated the suspension for 2 h. Next, we added 700 mL of NMP and shear mixed the sample at 5000 rpm for 4 h. The dispersion was sonicated again for 3 h and then shear mixed again for 1 h at 5000 rpm. The resulting suspension is shown in Figure 6a. The material was then centrifuged at 20 200*g* to yield a highly concentrated suspension of very thin, fractionated material (Figure 6a, small vial). In this suspension, nearly 25% of the sample was monolayers (Figure 6b) and the lateral size (Figure 6c) was similar to the material produced using bath sonication at a smaller scale (Figure 4). This demonstration reveals that the production of high-quality 2D phosphorus—including phosphorene—can be readily accomplished using simple and scalable approaches.

Optical Absorption in 2D Phosphorus: Background. The optoelectronic properties of black phosphorus and 2D phosphorus—high mobility, anisotropy, and the extreme variation in band structure with flake thickness—have provoked intense interest and debate. In 1981, a calculation first proposed the idea of a monolayer of black phosphorus[55] (*i.e.*, phosphorene) and calculated a band gap of 1.8 eV, which is significantly

larger than the bulk value of 0.33 ± 0.02 eV (see below for discussion). This remarkable prediction was dormant until several months ago, when the possibility of making phosphorene began to emerge. Despite this interest, the synthesis of monolayers has remained a challenge, and consequently, the majority of recent studies have been theoretical. These studies have essentially confirmed the 1981 prediction—that the band gap is tunable—although they have also introduced considerable uncertainty as to the actual size of the gap: values for monolayers typically range from 1.0 to 2.2 eV (see Table 1). Nevertheless, theory consistently predicts that the band gap is direct for all thicknesses of 2D phosphorus, which has driven further interest because most other 2D semiconductors have indirect band gaps.

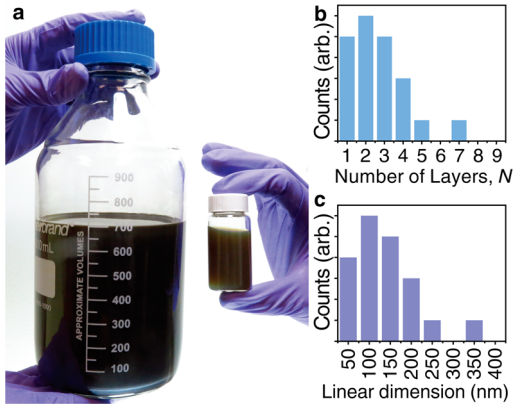

Figure 6. Scaled-up production of 2D phosphorus. (a) Photograph of solutions that were exfoliated using a combination of shear mixing and sonication. In our scale-up, we used 6 g of black phosphorus and 800 mL of NMP (left). We centrifuged 40 mL of this mixture at 20 200*g* to isolate a highly concentrated suspension containing thin pieces (right). The size distribution of 2D phosphorus in this fraction is shown in (b) and (c).

These predictions are compelling and need to be systematically examined, but so far, only a few experiments have been reported. Photoluminescence measurements have shown that these predictions are qualitatively correct, but with a varying exciton binding energy of 0.01 to 0.9 eV in phosphorene; this technique will underestimate the band gap of black phosphorus by a similar amount, which depends on the static dielectric constant of the surrounding medium.[56−58] In addition, surface defects, contamination, and oxidation of samples may introduce further experimental uncertainty. In fact, results so far are quite varied: in one study, a trilayer photoluminesced at 1.60 eV, while in another, the measured value was 0.97 eV (see optical gaps, Table 1). Electrical measurements have also been performed, and the reported mobility gaps were smaller than those found by photoluminescence (see mobility and optical gaps, Table 1), a result that is surprising because the mobility gap should be larger than the optical gap in a semiconductor with few interband states.[59,60] However, the study did provide a detailed analysis of many flake thicknesses and revealed that bulk properties begin to transition toward quantum-confined properties at flake sizes as large as 30 layers.[64]

In this section, we report our experiments on the optical absorbance of black phosphorus and fractionated suspensions of 2D phosphorus. We also report our analyses of these spectra, from which we estimate the absorption edge and band gap in black phosphorus and 2D phosphorus. Some of our analysis uses Elliot's theory of light absorption[68] by delocalized, Wannier-type excitons,[69] and we implement Elliot's theory in the form of Tauc plots.[70] Tauc plots determine the band-to-band transition energy as well as the nature of the transition—whether it is phonon-mediated (indirect) or not (direct), and whether it is dipole-mediated (allowed) or not (forbidden). A proper

TABLE 1. Reported Optical, Mobility, and Band Gaps of 2D Phosphorus

thickness (layers)	1	2	3	4	bulk	source
photoluminescence (optical gap, eV)	1.75	1.29	0.97	0.84		Yang[61]
	1.45					Liu[16]
	1.31					Wang[62]
		1.29	0.98	0.88		Zhang[63]
			1.60			Castellanos-Gomez[28]
electrical (mobility gap, eV)	0.98	0.71	0.61	0.56	0.30	Das[64]
computation (band gap, eV)	2.15	1.70	1.48	1.36	1.08	Castellanos-Gomez[28]
	2.0	1.30	1.06		0.30	Tran[37]
	1.94	1.7	1.3	0.8	0.43	Liang[65]
	1.60	1.01	0.68	0.46	0.10	Rudenko[66]
	1.52	1.01	0.79	0.67	0.36	Qiao[67]
	1.01	0.66	0.52	0.47	0.31	Liu[16]
		1.02	0.79	0.68		Zhang[63]
absorbance (band gap, eV)		1.88	1.43	1.19	0.33	this work (see Table 2)

Tauc plot yields a linear relationship between $(\alpha h\nu)^n$ and $h\nu$, where α is the absorption coefficient, $h\nu$ is the photon energy, and n describes the nature of the transition. Although Tauc plots have been criticized because of their simplistic assumptions about band structure and their poor treatment of excitonic effects,[56] they have been used to analyze the absorption edge of many semiconductors, including black phosphorus.[71] In a reported Tauc analysis of black phosphorus, a room-temperature band gap of 0.31 eV was found.[71] This agrees with previously reported electrical measurements,[17,72−76] which we have averaged to calculate a room-temperature band gap of 0.33 ± 0.02 eV. Although this agreement is promising, there are important differences between our 2D samples and bulk black phosphorus that may prevent the application of Tauc's method to our materials. Next, we consider these differences and the corresponding limitations of Elliot's theory.

We have identified five possible reasons why a Tauc analysis could fail to apply to our 2D phosphorus suspensions.

(1). Light Scattering. A Tauc analysis requires an accurate measurement of the absorption coefficient, α, *versus* wavelength. We measured light that is absorbed by our suspensions of 2D phosphorus using a transmission geometry, but in a traditional transmission geometry, most scattered light is not captured by the detector. To account for forward-scattered light, we placed samples near the opening aperture of an integrating sphere. This measurement showed that the amount of forward-scattered light was relatively small. In addition, because there is less back-scattered light than forward-scattered light,[77] we estimated that our measurements that capture both the transmitted and forward-scattered but neglect back-scattered light have less than a 3% error (see Supporting Information for complete details). Consequently, we have reported an absorption coefficient rather than an extinction coefficient.

(2). Exciton Binding Energy. Elliot's theory is only applicable to Wannier excitons, which have an exciton binding energy (EBE) of less than 100 meV. Bulk black phosphorus has an EBE of 8 meV, and the excitonic features in absorbance spectra are only apparent at low temperature.[17] The predicted EBE of phosphorene (a monolayer) depends on the static dielectric constant of the surrounding medium and can be as large as 900 meV in a vacuum.[28,37] We performed most optical absorbance experiments in NMP, which has a high dielectric constant (32.17) and yields a small EBE (15 meV; see Supporting Information). The small EBEs, combined with the measurement of our absorbance spectra at room temperature and low light intensities, allow Elliot's theory to be applied because excitons will not obscure the absorption edge as they do in MoS_2 and other transition metal chalcogenides.

(3). Urbach Tail. In materials with significant structural disorder, a pronounced absorption extends below the absorption edge.[78] This absorption, called an Urbach tail, could be present in 2D phosphorus because of the loss of periodicity and presence of defects at the edge of sheets. Urbach tails give a nonlinear contribution to Tauc plots. To avoid misinterpreting our spectra, we only extracted an estimate of the band gap when a linear fit of the Tauc plot was obtained at energies above the Urbach tail.

(4). Anisotropic Optical Properties. The nature of black phosphorus' band gap depends on direction: it is direct and allowed in the *c* direction but direct and forbidden in the *a* direction (see Figure 1b).[17] In principle, this would prevent a Tauc plot from distinguishing either transition. Fortunately, the forbidden transition is relatively weak, and its contribution to light absorption is negligible;[17] thus, it does not obscure the Tauc analysis of the direct, allowed band gap.

(5). Variation in Band Gap. Tauc analyses are typically applied to materials with a single band gap. If multiple gaps are present and they span a narrow range of energies, it is not possible to distinguish each gap. The superposition of multiple absorption edges of similar strength leads to nonlinearity in the Tauc plot, preventing one from determining the nature of the absorption edge or from extracting an accurate band gap energy. Of the five limitations, we found that this consideration is the most important. Our suspensions contain flakes of several thicknesses and therefore several band gaps. Because the absorption coefficients from flakes of different thicknesses are similar and because their band gaps fall across a range of energies, we found that it is not always possible to use a Tauc analysis (see below). In those instances, we have developed and applied a different method for estimating the absorption edge.

Optical Absorption in 2D Phosphorus: Measurement and Tauc Analysis. In this section, we report our measurement and Tauc analyses of the optical absorbance of 2D phosphorus suspensions. In order to interpret these measurements, we first established reference spectra of bulk black phosphorus. We performed UV−vis−NIR (175−3300 nm) and FT-IR measurements on a polycrystalline sample (KBr pellet, Figure 7a, black) and used a CRAIC microspectrophotometer on single flakes of mechanically cleaved bulk crystals (Figure 7a, gray). All spectra were acquired under an inert atmosphere. Fractionated suspensions of 2D phosphorus (Figure 4) were analyzed using an integrating sphere to capture both transmitted and scattered light (see Supporting Information for full experimental details).

The polycrystalline black phosphorus within the KBr pellet had a high optical density, which allowed us to quantify light absorption near the band gap threshold. We observed an onset of absorption at *ca.* 0.4 eV (Figure 7a, black), characteristic of bulk black phosphorus. The analysis of cleaved phosphorus flakes

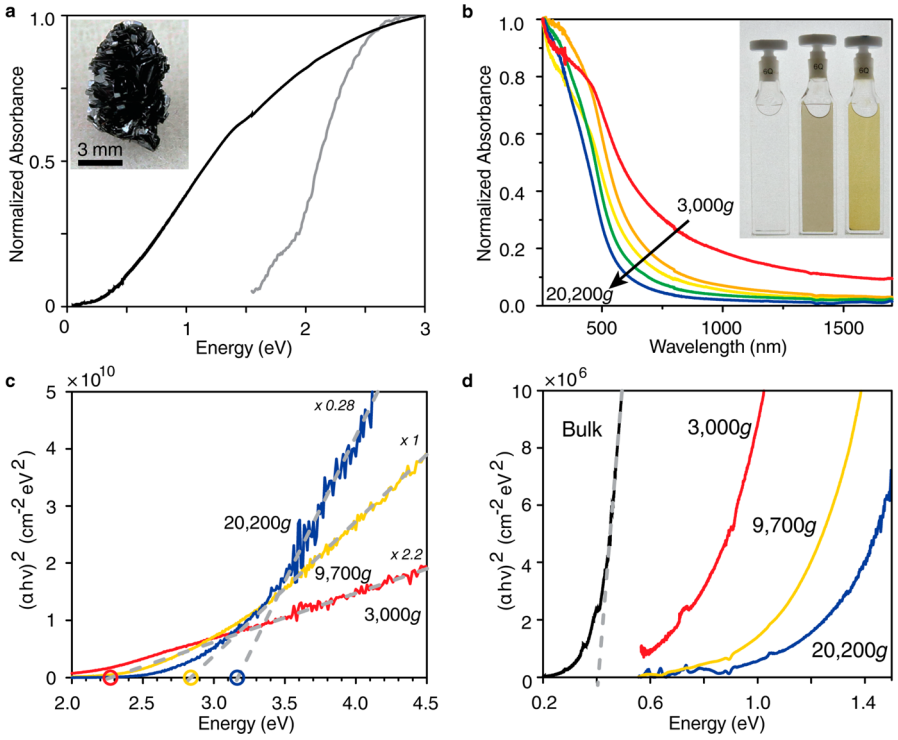

Figure 7. UV−vis−NIR spectroscopy of black phosphorus and its liquid-exfoliated few-layer flakes. (a) Optical absorbance of bulk phosphorus measured at two different optical densities (black = high; gray = low) to reveal two distinct optical transitions (*ca.* 0.4 and 1.95 eV). (b) Absorbance of 2D phosphorus suspensions that were prepared by fractionation at rcf values near 3000, 5900, 9700, 14 500, and 20 200*g* (red to blue). (c) Representative direct Tauc plots used to determine the high-energy band-to-band transition. (d) Representative direct Tauc plots of the low-energy optical transition. The fit to Tauc models is poor, consistent with the wider range of optical absorption edges that are present in these suspensions.

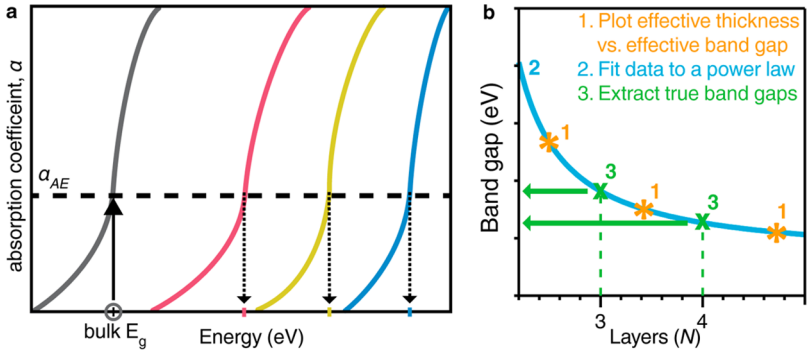

Figure 8. "Alpha method" for band gap determination. (a) Absorption coefficient at the absorption edge (α_{AE}) is measured for the bulk material. We use this α_{AE} to estimate the band gap energy for the quantum-confined 2D flakes. If the 2D flakes are not monodisperse in thickness, the band gap that we have determined is an effective band gap. (b) To convert an effective band gap into a real band gap, we (1) plot the effective band gap *vs* effective thickness for a series of polydisperse samples. Next (2), we fit the data to a power law, see eq 1 in the text. Last (3), we use the power-law fit to extract the band gap for 2D flakes with real thicknesses.

(20−40 nm thick) with low optical density revealed an additional absorption edge at *ca.* 1.95 eV (Figure 7a, gray). We attribute this absorption event to a higher energy transition. We will see that these two absorption thresholds—the low-energy band gap transition and the high-energy transition (see band diagram in Figure 8b)—are also present in suspensions of 2D phosphorus.

The fractionated suspensions of 2D phosphorus varied significantly in their appearance: in transmitted light, dilute suspensions of thick pieces appeared black or brown while those containing primarily thin pieces appeared red or yellow (Figure 7b, inset). These observations were consistent with the corresponding optical absorbance spectra of the suspensions (Figure 7b), in which we observed a spectral blue shift as the flake thickness decreased. There are two notable features in these spectra: a sharply rising absorption within the visible region and a slowly rising absorption that extends into the near-IR. In the following analysis, we will attribute these spectral features to the same high- and low-energy transitions observed in the bulk material.

We sought to quantify these absorption features by using a Tauc analysis. The high-energy transition achieved an excellent fit to a Tauc model when $n = 2$, indicating that this transition is direct and allowed (Figure 7c). We assigned the high-energy transition energies to values of 1.95 eV in bulk black phosphorus and 3.15 eV in a suspension containing primarily monolayers, the thinnest fraction analyzed. The fact that the Tauc models fit our data may suggest that the five experimental challenges outlined above—light scattering, high exciton binding energy, Urbach tail, anisotropic optical properties, and variation in band gap—have a negligible effect on our Tauc analyses of the high-energy transition.

When we applied the direct Tauc model to the low-energy transition, we measured a value of 0.40 eV for bulk black phosphorus (Figure 7d, bulk), which is slightly larger than previous estimates of its band gap. The method of sample preparation—grinding bulk black phosphorus with KBr to make a pellet—may have exfoliated some thin sheets, yielding a slightly larger band gap. We found that the band gap is direct and allowed, which is consistent with earlier findings. Because theory consistently predicts that the band gap is direct for all thicknesses of 2D phosphorus, we attempted to apply direct Tauc models (both allowed and forbidden) to the low-energy, band gap transition of 2D phosphorus. For all Tauc models that we explored, we never found a linear region of the Tauc plot, which prevented us from determining the band gap using this method (Figure 7d shows the direct, allowed Tauc plot). We attribute the nonlinearity of the Tauc plot to several causes. First, the low-energy transition has a lower absorption coefficient than the high-energy transition. The weak absorbance is more likely to be obscured by other optical processes, such as light absorption from Urbach tails or light scattering. Second, the polydispersity of our samples gives a broader distribution of absorption edges for the low-energy absorption than for the high-energy absorption. This is because the high-energy transition is less sensitive to flake thickness than the low energy transition, as will become apparent in the following analysis. Because of these experimental challenges in applying a Tauc analysis to the absorption edge of 2D phosphorus, we introduce a new analytical method that can supplant the Tauc method when analyzing families of bulk and quantum-confined semiconductors.

Method for Determining Absorption Edges in Quantum-Confined Semiconductors. In our suspensions of 2D phosphorus, sample polydispersity has prevented a straightforward application of Elliot's theory. Indeed, this is an extremely common problem, and the liberal application of the Tauc method often causes large errors in the measurement of band gaps.[56] To circumvent these challenges, we now introduce an alternate method that can be applied to families of bulk and quantum-confined semiconductors such as black and 2D phosphorus. We validated our method using simulated absorption spectra of monodisperse and polydisperse suspensions of 2D phosphorus. Our tests demonstrate that the method is robust: it can determine absorption edges of semiconductors in polydisperse samples and has several advantages over the Tauc method, such as providing an estimate of uncertainty in the absorption edge energy (usually less than a few percent). Crucially, the measurement of an absorption edge (also called the optical gap) also allows us to determine the band gap because the optical and band gaps differ in energy by the exciton binding energy, which is <15 meV in our experiments and therefore negligible.

Our analytical method, which we call the "alpha method", utilizes the similarities that often exist between the electronic structures of quantum-confined semiconductors and the corresponding bulk semiconductor. As an example, numerous studies of black phosphorus and 2D phosphorus show that the band gaps of bulk and 2D phosphorus are always direct with both allowed and forbidden contributions, that their lowest energy transition is always located at the *Z*-point (in a 3D Brillouin zone), and that the conduction and valence bands are always comprised primarily of p_z orbitals.[17,37,55] In the case of the black phosphorus family, these similarities result in joint densities of states near the absorption edge that are virtually unchanged among members of the family, except for an effective scissoring of the band gap energy. In general, the absorption coefficient increases with increasing quantum confinement,[79] but we hypothesized that the change in the absorption coefficient at the absorption edge (α_{AE}) with confinement would be small and could therefore be treated as being unchanged from the bulk to the monolayer. While this is an oversimplification, we will show that this introduces only a small error in the determination of optical/band gap energies.

The stepwise analytical method that follows from this hypothesis is illustrated in Figure 8a. Using black phosphorus as an example, we exploit the fact that the band gap of the bulk material has been measured many times and has a well-defined value (0.33 ± 0.02 eV). First, we measure the absorption spectrum of the bulk material to determine the value of α_{AE}. Second, we measure the absorption spectra of a series of samples of 2D phosphorus. Finally, we assign the band gap of each sample as the energy at which the absorption coefficient equals α_{AE} (see Figure 8a). Note that this process is equating the absorption edge (optical gap) and the fundamental absorption edge (band gap), which is an accurate approximation in our experiments but is not necessarily true in all cases.

To validate the alpha method, we used four calculated (G_0W_0) absorption spectra—the spectra that come from bulk, trilayer, bilayer, and monolayer phosphorus.[37] For each spectrum, we used the reported band gaps, acquired by measuring the energy difference

between the conduction and valence bands. We then applied the alpha method to the same data to obtain a second estimate. Across this family of materials, we found that the maximum difference between the methods was 1.85%—an amount that is essentially negligible for most purposes (see Supporting Information for a complete analysis). Although the central assumption—that α_{AE} is the same in all members of the family—is not true, the error due to this assumption is small. This is because α rises steeply near the band gap ($d\alpha/dE$ is large as the energy E approaches the band gap energy E_g). Consequently, even if large differences in α_{AE} exist among the members of a semiconductor family, these produce small differences in the estimated band gap energy.

With this set of results for monodisperse samples in hand, we then tested whether the alpha method could be applied to polydisperse samples. We constructed a series of 24 different artificial mixtures of two-, three-, four-, and five-layer pieces by taking linear combinations of the calculated absorption spectra of the individual flakes. For these mixtures, Tauc plots were often unusable: the plots either contained several linear regions or did not contain any linear region at all. On the other hand, when we applied the alpha method to each suspension, we always obtained an estimate of an "effective band gap". We found that the effective band gap increased monotonically as the sample distributions shifted from containing a majority of thicker flakes (four or five layers) to a majority of thinner flakes (two or three layers) and that, as expected, the effective band gap always fell between the band gaps of the thinnest (two-layer) and thickest (five-layer) flakes. This example shows that the effective band gap does not necessarily correspond to the band gap of any real material but rather represents the contributions from various-sized flakes in a given mixture. Nevertheless, if this effective band gap is properly correlated with an "effective thickness" and these band gap thickness correlations are performed on multiple samples, then it would be possible, at least in principle, to interpolate between these data points to obtain the band gap of 2D materials with real thicknesses (*e.g.*, a bilayer or a trilayer), as illustrated in Figure 8b.

The challenge with this approach is that it is not obvious whether the interpolated values are correct. We addressed this challenge by applying a robust mathematical approach to determine an effective thickness for each simulated mixture that, when paired with the effective band gap (alpha method), would lead to correct values of the band gap for real flake thicknesses. We compared our effective thicknesses and effective band gaps to those predicted by a power-law fit of the true thickness and true band gaps for the individual flakes in our simulated mixtures. A power-law fit was selected because, as suggested by numerous calculations, it appears to correctly describe the variation in band gap with flake thickness.[16,28,37,67,80] The power-law model yields a band gap for the Nth layer as

$$E_{g_N} = \frac{E_{g_1} - E_{g_\infty}}{N^x} + E_{g_\infty} \quad (1)$$

where E_{g_1} is the band gap of phosphorene (a monolayer), E_{g_∞} is the band gap of bulk black phosphorus, and x is a parameter describing the nature of quantum confinement in the system. Values of x are usually between 0 and 2, where the variation is due in large part to the extent of Coulomb interactions[79,81] and therefore depends on the material geometry (quantum dot *vs* nanowire *vs* 2D flake). In the present case, the power-law fit is useful because it provides an excellent fit to the calculated G_0W_0 spectra and because it allows us to make direct comparisons of the real band gaps to the effective band gaps at nonreal (*i.e.*, noninteger) thicknesses.

In these calculations, we considered the same series of mixtures as above. The skewness of these 24 distributions was systematically varied to capture the full range of likely skews that may be observed experimentally, which, as seen in Figure 4, typically have a log-normal shape. For each artificial mixture, we employed the alpha method to determine an effective band gap, and we tested five different statistical approaches to extract effective thicknesses. The approaches that we tested were a number-averaged mean (analogous to $\overline{M_n}$ in polymer physics), a weight-averaged mean (analogous to $\overline{M_w}$ in polymer physics), and the mean, median, and mode that were derived from a log-normal fit to each distribution. We note that the weight-averaged mean is not equivalent to a weight fraction, which is defined as the weight of material per total weight of solvent and material (see Supporting Information, section 12, for a complete description of these statistical measures).

From these 24 mixtures comprising realistic skews, we found that the best two averages were the log-normal mean and the number-averaged mean. When paired with the effective thickness as calculated by the log-normal mean, the calculated band gap (power law) was 0.3 $\pm$ 1.5% above the effective band gap (alpha method). When paired with the effective thickness from the number-averaged mean, the calculated band gap was 0.2 $\pm$ 2.6% below the effective band gap. The next two closest measures of thickness were the log-normal median (2.3 $\pm$ 1.6% above the effective band gap) and the weight-averaged mean (3.6 $\pm$ 3.5% below the effective band gap). In general, we found that the extent to which these statistical measures over- or underestimated the true band gap varied systematically with the skewness of the distribution. For distributions with low skewness, the band gap was systematically overestimated by about 1.5%, while for

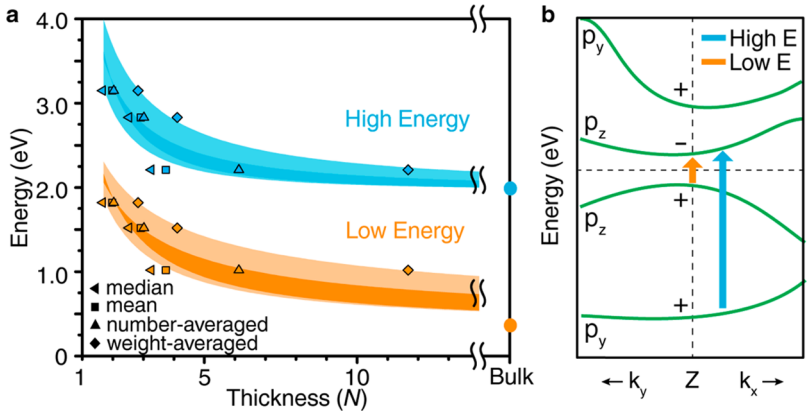

Figure 9. Experimentally determined band gap (low energy) and high-energy transitions of 2D and bulk black phosphorus. (a) Band gap (orange, "low energy") and high-energy band-to-band (blue, "high energy") transitions are plotted with respect to flake thickness. The dark blue and dark orange regions define the most probable energy values, and the light orange and light blue regions define the maximum likely range. (b) Band structure of bulk black phosphorus at the *Z*-point of the first Brillouin zone. The orange arrow represents the band gap transition (VB → CB), and the blue arrow represents the high-energy transition (VB−1 → CB). The plot also shows the parity of bands near the *Z*-point (+, −) and the nature of orbitals that primarily contribute to each band (p_y, p_z). The valence bands come from angle-resolved photoelectron spectroscopy measurements,[18,83] and the conduction bands come from calculations.[18,67] The horizontal dashed line shows the Fermi level.

distributions with high skewness, such as those obtained in our experiments (Figure 4), the band gap was systematically underestimated by about 1%, although there were a small number of outliers with errors up to 6%. A table and graphs that summarize these calculations are provided in section 12 of the Supporting Information.

The central conclusion from these simulations is that the alpha method, when combined with an appropriate flake thickness, yields band gaps that are reliable. As noted above, the maximum difference between the reported band gap and the alpha band gap was 1.85%. In addition, the maximum error in using either the number-averaged mean or the log-normal mean was 6%. We emphasize that these are maximum errors and the typical errors will be less. However, these estimates of error only describe those errors due to data analysis and do not include systematic or nonsystematic errors that are inherent to the experimental measurements.

Thickness-Dependent Absorption Edges of Black and 2D Phosphorus. In this section, we compile the results of our experimental determination of the absorption edge of 2D phosphorus. As we described above, the absorption edge probed by our experiments (the optical gap) is indistinguishable from the band gap because the exciton binding energy is extremely small (8−15 meV), and exciton fission is rapid. When discussing the energy associated with a particular transition, we will use "absorption edge", "optical gap", and "band gap" interchangeably.

From the absorption spectrum of bulk black phosphorus, we measured α_{AE} to be 0.24 μm^{-1}, which is equivalent to a light penetration depth of 4 μm. (We note that the absorption coefficient determined by us is similar to the one reported previously,[73] $\alpha_{AE} = 0.17\ \mu m^{-1}$.) We then used this absorption coefficient to determine the effective band gap of each 2D phosphorus suspension. The thickness distribution of each phosphorus suspension was analyzed by TEM, and this distribution was converted into effective thicknesses using the four most accurate statistical averages (log-normal mean, number-averaged mean, log-normal median, and weight-averaged mean). For each of these averages, a power law (eq 1) was fit to the thickness band gap data set. The same process was repeated for the high-energy transition, with the only difference being that the band-to-band transition energy was taken from a Tauc analysis rather than the alpha method (see justification above).

Figure 9 summarizes our most important findings: the experimental quantification of the band-to-band transitions of 2D phosphorus. Figure 9a displays the band gaps (orange curves, "low energy") and high-energy transitions (blue curves, "high energy"). The low-energy and high-energy transitions show the most probable values (dark orange, dark blue) and a maximum likely range of values (light orange, light blue). The four curves that define the most probable and maximum likely boundaries come from the power-law fits to the four types of effective thicknesses, with the most probable boundaries defined by the log-normal and number-averaged means and with the maximum likely boundaries defined by the log-normal median and weight-averaged mean. The average exponent *x* of the power law (eq 1) calculated from our data is 0.81. Earlier theoretical predictions suggest that the value may be between 0.7 and 1.0, with an average value of 0.80 ± 0.11 reported across six studies.[16,28,37,67,82]

Our measurements provide direct experimental evidence that the band gap and the high-energy transitions undergo extreme changes as flakes

TABLE 2. Electronic Band-to-Band Transitions in 2D Phosphorus

layers	band gap (eV)	high energy (eV)
2	1.88 ± 0.24	3.23 ± 0.39
3	1.43 ± 0.28	2.68 ± 0.32
4	1.19 ± 0.28	2.44 ± 0.27
5	1.04 ± 0.27	2.31 ± 0.23
6	0.94 ± 0.26	2.23 ± 0.20
7	0.87 ± 0.26	2.18 ± 0.17
8	0.81 ± 0.25	2.14 ± 0.16
9	0.77 ± 0.24	2.11 ± 0.14
10	0.73 ± 0.23	2.09 ± 0.13
15	0.62 ± 0.20	2.03 ± 0.09
20	0.56 ± 0.18	2.01 ± 0.07
∞	0.33 ± 0.02	1.95 ± 0.06

approach monolayer thickness. The band gap can be tuned from 0.33 ± 0.02 eV in bulk to 1.88 ± 0.24 eV in bilayers. The higher energy transition can be tuned from 1.95 ± 0.06 eV in bulk to 3.23 ± 0.39 eV in bilayers. These ranges surpass all known 2D materials and are as large as the most tunable quantum dots. The most important band gaps and high-energy transitions are reported in Figure 9a and Tables 1 and 2. Our estimates of error (*e.g.*, ±0.24 eV for the band gap of bilayers) are the same as the maximum ranges in Figure 9a (light blue and light orange regions). These estimates of error do not include the 1.85% maximum error between the alpha method and reported gaps or experimental error. We have not extrapolated our power law to a monolayer thickness because of the errors associated with such an extrapolation: the smallest effective thickness of our samples was 1.71 layers, and it has also been suggested that a phosphorene monolayer does not lie on the power-law curve.[37]

In order to place these measurements in context, we compare our band gaps to prior optical gap measurements (see Table 1). We focus, in particular, on the optical gaps of Yang[61] and Zhang[63] because these studies surveyed the largest range of flake thicknesses and because these studies are the only two that are in agreement. When the optical gap and band gap are measured in the same dielectric environment, the band gap is expected to be larger than the optical gap by an amount equal to the exciton binding energy. This relationship only holds true for measurements that are performed in media with the same dielectric constant because the exciton binding energy, optical gap, and band gap all depend on the medium's dielectric constant. This sensitivity to the medium's dielectric constant disappears as flakes become thicker, and in the limit of thick flakes, the optical gaps and band gaps converge because the exciton binding energy is 8 meV in bulk black phosphorus.[17] To see whether the electrical gap and optical gap do converge, we focus on four- and five-layer thicknesses, which are the thickest flakes that have been studied in the photoluminescence (optical gap) experiments. The four-layer optical gap was reported as 0.86 eV, and the five-layer optical gap was 0.80 eV. We measured a four-layer band gap as 1.19 ± 0.28 eV and a five-layer band gap as 1.04 ± 0.27 eV. It is apparent that the difference between the band gap in our experiments and the optical gap in the photoluminescence experiments is decreasing (0.33 eV for four-layer, 0.24 eV for five-layer), as expected. Although the extent to which we can make comparisons is limited by the available data, it appears that there is reasonable agreement between our measurements and some previous photoluminescence measurements.

Next, we turn our attention to the high-energy band-to-band transition. Although this transition has been neglected in earlier studies, we suggest two reasons that understanding this transition will be important. First, the changes in the color of 2D phosphorus with decreasing thickness (Figure 7b, inset) are due, in large part, to changes in the high-energy band-to-band transition rather than the band gap. As a result, the ability to modulate the material's color requires an understanding of the high-energy transition. Second, the high-energy transition has a substantially larger absorption coefficient (3.3 μm^{-1} at 3 eV) and a smaller light penetration depth (300 nm at 3 eV) than the band gap transition. This feature will be important in designing 2D phosphorus for applications that require high light absorption. From our Tauc analyses of the high-energy transition, we found that the bulk material has a transition energy of 1.95 eV, increasing up to 3.23 ± 0.39 eV in bilayers (Figure 9b, blue). From these measurements, it is also apparent that the high-energy transition is less sensitive to flake thickness compared to the low-energy band gap transition: from bulk to bilayers, the band gap changes by 1.55 eV, while the high-energy transition changes by 1.28 eV. This difference in sensitivity may be why Tauc plots appear to work well for the high-energy transition, while they do not work for the low-energy transition.

Finally, we describe four key observations that allow us to determine the nature of the high-energy transition. First, the Tauc plots show that there is a linear relationship between $(\alpha h\nu)^2$ and the photon energy (Figure 7c), which is characteristic of a direct, allowed transition. Second, the high-energy transition is sensitive to material thickness, varying from 1.95 eV in bulk to 3.23 eV in bilayers. These changes follow a power law and therefore appear to be driven by quantum confinement.[79,81] As such, it is plausible that the high-energy transition occurs at or near the *Z*-point of the Brillouin zone because *Z* is perpendicular to the plane of flakes. In examining the band structure near the *Z*-point (Figure 9b), it is clear that there are two likely candidates for a direct optical transition at or near the *Z*-point: a transition between the valence band (VB) and the second lowest unoccupied band (CB+1) or

between the second highest occupied band (VB−1) and the conduction band (CB). Third, the energy of the transition for the bulk material (1.95 eV) can be compared to previous measurements of the band structure of bulk black phosphorus.[15,83] From these comparisons, it is clear that only the VB−1 → CB transition provides the right energy. Fourth, the absorption coefficient of the high-energy optical transition is considerably larger (about 10 times larger) than that of the low-energy optical transition. This observation is consistent with an assignment of the optical transition to VB−1 → CB: this transition is direct, allowed in the *c*-direction, and leads to a change in parity (+ → −).[17] These selection rules favor strong optical absorption. Figure 9b summarizes this assignment and also identifies the low-energy transition.

CONCLUSIONS

In this work, we have described our method[42] for preparing and isolating large quantities of monolayers, bilayers, and few-layer flakes, and we identified benzonitrile as the best solvent of those we surveyed. Although shear mixing provides insufficient force for exfoliating high-quality samples of black phosphorus, it is possible to combine shear mixing and sonication to exfoliate black phosphorus at the 10 g scale. Using XPS, TEM, and multislice TEM simulations, we observed that monolayers, bilayers, and few-layer flakes of 2D phosphorus are crystalline and unoxidized. Our work also demonstrates a rapid and simple TEM-based method for measuring the thickness of 2D phosphorus.

Using a method that we introduced here for quantifying the optical absorbance spectra, we showed that it is possible to measure the optical gap of polydisperse 2D phosphorus samples and to extract an accurate estimate of the material's band gap. Our results may go some ways toward resolving the long-standing question of how the band gap of black phosphorus changes with thickness. We expect that the methodology presented here will be broadly applicable as it provides a robust approach for optical or band gap measurement in mixtures of complex semiconductors and can extract useful information even when the Tauc analysis fails.

Of central importance for future applications of 2D phosphorus, we have performed the first accurate measurements of the thickness-dependent band gap. Although there are a large number of theoretical predictions, these predictions have not yet been tested, until now, by careful experiments. We found that the band gap can be tuned from 0.33 ± 0.02 eV in bulk black phosphorus to 1.88 ± 0.24 eV in bilayer phosphorus. It is important to note that the band gap will likely depend on the surrounding medium, but in any case, the range of optical transitions for black and 2D phosphorus is relatively large compared to that of other quantum-confined nanomaterials such as MoS_2 (1.2−1.9 eV),[9,84] CdSe quantum dots (2.0−3.0 eV),[85] or PbSe quantum dots (0.27−1.5 eV).[11−13] This suggests that the electronic coupling between layers is stronger than in most other van der Waals layered solids, but a complete description of this unusual property is still needed. Looking toward future applications of this material, we suggest that the astounding range of band gaps that can be achieved by 2D phosphorus, with tunable absorption thresholds from the infrared to the visible, will provide a new material platform for the design and development of solar cells, photodetectors, photocatalysts, transistors, and batteries.

METHODS

Chemicals. All chemicals were purchased from Sigma-Aldrich unless otherwise noted: black phosphorus (Smart Elements, ~99.998%), red phosphorus (≥99.999+%), *N*-methyl-2-pyrrolidone (Sigma-Aldrich or Acros Organics, anhydrous, 99.5%), 2-propanol (FisherSci, electronic grade), cyclopentanone (≥99%), 1-cyclohexyl-2-pyrrolidone (≥99%), 1-dodecyl-2-pyrrolidinone (≥99%), benzyl benzoate (≥99.0%), 1-octyl-2-pyrrolidone (≥98%), 1-vinyl-2-pyrrolidinone (≥99%), benzyl ether (≥98%), 1,3-dimethyl-2-imidazolidinone (≥99%), cyclohexanone (≥99.8%), chlorobenzene (≥99.5%), dimethyl sulfoxide (≥99.9%), benzonitrile (anhydrous, ≥ 99%), *N*-methylformamide (≥99%), dimethylformamide (≥99%), benzaldehyde (≥99%). The solvents were degassed prior to use, handled under nitrogen in a glovebox (O_2 < 1 ppm), and transferred from instrument to instrument using custom-designed glassware with Rotaflo stopcocks. When necessary, instrument loading chambers or entire instruments were enclosed in N_2-filled glove bags to provide an inert atmosphere.

Synthesis. Black phosphorus was purchased from Smart Elements or made in our laboratory using a method similar to that of Nilges.[46] Red phosphorus (0.5 g), tin (10 mg), and tin iodide (15 mg) were loaded into a partially sealed quartz tube in a glovebox. The tube was 14 cm long, with a 1 cm inner diameter and a 1.4 cm outer diameter. The tube and its contents were evacuated to *ca.* 4×10^{-3} mbar and sealed with an oxyhydrogen torch while maintaining vacuum within the ampule. We ensured that the ends of the quartz tubes were >0.4 cm and without entrapped gas bubbles; in one experiment, the quartz tube burst because the walls were too thin. (Caution: only perform this synthesis in a well-ventilated area with restricted access as the risk of unanticipated explosions is high because the tube pressure greatly exceeds 1 atm.) The reaction was carried out in a Lindberg Blue three-zone furnace using the temperature profile described by Nilges. We maintained a 60 °C temperature differential across the 15 cm tube by inserting insulation between the two zones. The tube was opened in our glovebox, and the reaction products were washed sequentially in anhydrous acetone, *N*-methyl-2-pyrrolidone, and isopropyl alcohol and subsequently dried prior to use.

Liquid Exfoliation. Black phosphorus crystals were ground into granular pieces using a mortar and pestle in a nitrogen glovebox. For typical experiments, 10 mg was added to a 20 mL scintillation vial. Twenty milliliters of solvent was added to give a concentration of 0.5 mg/mL. Vials were tightly capped and wrapped with parafilm to prevent air exposure before placing into a Branson 5800 bath sonicator. The bath sonicator was outfitted with a test tube rack to allow for controlled placement of vials. Vials were systematically moved through several locations during the course of sonication to minimize vial-to-vial variations in phosphorus dispersion. The samples were subjected

to eight to 10 cycles of sonication at high power, each lasting 99 min. Bath water was changed after each cycle to maintain a temperature between 22 and 30 °C (during sonication, bath temperature increased dramatically). During the sonication process, the black phosphorus crystals dispersed into the solution and the suspension acquired a brown appearance. After sonication, the vials were returned to the glovebox.

Centrifugation. Centrifugation was performed in a Sorvall RC-5B superspeed refrigerated centrifuge with a rotor radius of 10.7 cm. Dispersions of sonicated black phosphorus were transferred into Nalgene Oak Ridge FEP 10 or 50 mL centrifuge tubes. We list centrifuge speed as rcf (relative centrifugal force) rather than rpm (revolutions per minute) because rpm alone provides an incomplete description of centrifugation conditions. See Supporting Information for more details on sample handling and procedure.

Transmission Electron Microscopy. A JEOL 100CX II TEM was used for low-resolution imaging at a 100 kV accelerating voltage with a resolution of 2 Å (lattice) and 3 Å (point-to-point). For HR-TEM, we used a JEOL 2010F-FasTEM at 200 kV accelerating voltage for a resolution of 1 Å (lattice) and 2.3 Å (point-to-point). Samples were prepared in a glovebox, where the phosphorus dispersion (in IPA or NMP) was drop-cast (~10 μL) onto a 300-mesh copper TEM grid coated with lacey carbon (Ted Pella). After deposition, the solvent was evaporated for 1 h (IPA) or at least 48 h (NMP). During this period, TEM grids were held with self-closing tweezers and were not blotted against filter paper to ensure that a representative distribution of the material was deposited. The TEM grids were placed in a grid box wrapped in aluminum foil, placed in a nitrogen-filled zip-loc bag, and brought to the TEM. Grids were rapidly transferred into the TEM with a minimal amount of light exposure. For both TEM analyses, images were acquired and processed with Gatan digital micrograph. Fast Fourier transforms were applied to HR-TEM images to observe the plane families present in the HR-TEM images of phosphorus flakes.

Edge Contrast Analysis. We performed this analysis with the line profilometer tool of Gatan digital micrograph software. The lateral dimensions of each flake are reported as the diagonal of two perpendicular length measurements. See Supporting Information for full description.

Multislice Calculations. To simulate HR-TEM images of 2D phosphorus from one to eight layers, we used Java electron microscopy software (JEMS) version 4.1830U2014 by Pierre Stadelmann.[47] Multislice calculations were performed using four HR-TEMs including a JEOL 2010 LaB6 with a UHR or HRP pole piece, a CM 300 SuperTwin, a JEOL 2100-non C_s-corrected TEM, and a Titan 80-300. Crystallographic information files were created using Accelrys' Materials Studio and then imported to JEMS for image simulation through a range of defocus values near Scherzer defocus for each TEM. FFTs were applied to the simulated images to generate the {101}, {200}, and {002} plane families. We used image integration techniques to measure spot intensities in the FFTs.

X-ray Photoelectron Spectroscopy. XPS data were taken with a Kratos Axis Ultra DLD spectrometer with a monochromatic Al Kα X-ray source. High-resolution elemental scans were taken with a pass energy of 20 eV. Although a charge neutralizer was used for the measurement of bulk black phosphorus, charging inconsistencies of the C 1s peak prevented correction of the elemental P 2p peak to the C 1s peak. The 2D samples showed much less charging than the bulk samples, and energy correction with the C 1s peak (284.6 eV) was possible. Unless otherwise noted, all preparation was performed inside a nitrogen-filled glovebox and transported to the XPS chamber in custom glassware. All sample transfers into/from the XPS chamber utilized a nitrogen-purged glovebag to prevent premature oxidation by air and/or water vapor. The XPS loading chamber was vented with N_2. The black phosphorus samples (bulk) were mechanically cleaved using carbon or copper double-sided tape to expose a fresh (nonoxidized) surface; the tape was also used as a substrate for these experiments. Samples were subsequently removed from the XPS chamber and exposed to ambient air and room light for controlled periods of time. After air exposure, samples were loaded into the XPS and a phosphorus oxide peak was observed. The cycle was repeated over several iterations, and growth of the oxide peak was quantitatively measured in relation to the elemental P 2p peak.

UV−Vis−NIR Spectroscopy. All spectroscopy was performed on a Cary 5000 double-beam spectrometer with an external integrating sphere apparatus. Starna 1 mm path length quartz cuvettes with transparency range from 170 to 2700 nm were used in all experiments. Cuvettes were filled in a glovebox and fitted with airtight PTFE stoppers to maintain an inert atmosphere. See Supporting Information, section 10, for a more detailed description. Concentration of suspended flakes was determined by correlating UV−vis data with ICP-MS. Samples were prepared in NMP, centrifuged at 3000*g*, and dialyzed into fresh NMP under inert conditions to remove possible molecular phosphorus byproducts caused by sonication (Millipore Biotech RC membranes, 8−10 kDa). See Supporting Information for more details.

Conflict of Interest: The authors declare the following competing financial interest(s): Several authors are patenting the method of liquid exfoliation described herein.

Supporting Information Available: The Supporting Information is available free of charge on the ACS Publications website at DOI: 10.1021/acsnano.5b02599.

Full description of synthesis, characterization, and modeling (PDF)

Acknowledgment. S.C.W. acknowledges support of this research by UNC Chapel Hill startup funds, the UNC Office of Technology Development, and the National Science Foundation under Grant DMR-1429407. T.W.F. and A.H.W. acknowledge support of this work by the National Science Foundation Graduate Research Fellowship under Grant No. DGE-1144081. Any opinion, findings, and conclusions or recommendations expressed in this material are those of the authors(s) and do not necessarily reflect the views of the National Science Foundation. We thank Bruker Instruments for access to a FastScan AFM. We thank J.F. Cahoon and group members for access to furnaces, sonicators, and other equipment while our laboratory was built. We thank A.S. Kumbhar for assistance in HR-TEM imaging. We acknowledge P. Stadelmann, E. Samulski, J. DeSimone, J.F. Cahoon, K.L. Kuntz, D. Druffel, and S. Kolavennu for fruitful discussions. We thank T. Nilges and M. Köpf for sharing the details of their black phosphorus synthesis[46] prior to publication. A portion of this work was performed in the UNC-EFRC Instrumentation Facility established by the UNC EFRC (Solar Fuels and Next Generation Photovoltaics, an Energy Frontier Research Center funded by the U.S. Department of Energy, Office of Science, Office of Basic Energy Sciences under Award Number DE-SC0001011) and the UNC SERC ("Solar Energy Research Center Instrumentation Facility" funded by the U.S. Department of Energy, Office of Energy Efficiency & Renewable Energy, under Award Number DE-EE0003188).

REFERENCES AND NOTES

1. Thompson, B. C.; Fréchet, J. M. J. Polymer-Fullerene Composite Solar Cells. *Angew. Chem., Int. Ed.* **2008**, *47*, 58–77.
2. Talapin, D. V.; Murray, C. B. PbSe Nanocrystal Solids for N- and P-Channel Thin Film Field-Effect Transistors. *Science* **2005**, *310*, 86–89.
3. Wu, J.; Agrawal, M.; Becerril, H. A.; Bao, Z.; Liu, Z.; Chen, Y.; Peumans, P. Organic Light-Emitting Diodes on Solution-Processed Graphene Transparent Electrodes. *ACS Nano* **2010**, *4*, 43–48.
4. Rossetti, R.; Nakahara, S.; Brus, L. E. Quantum Size Effects in the Redox Potentials, Resonance Raman Spectra, and Electronic Spectra of CdS Crystallites in Aqueous Solution. *J. Chem. Phys.* **1983**, *79*, 1086.
5. Brus, L. Electronic Wave Functions in Semiconductor Clusters: Experiment and Theory. *J. Phys. Chem.* **1986**, *90*, 2555–2560.
6. Rossetti, R.; Hull, R.; Gibson, J. M.; Brus, L. E. Excited Electronic States and Optical Spectra of ZnS and CdS Crystallites in the ~ 15 to 50 Å Size Range: Evolution from

Molecular to Bulk Semiconducting Properties. *J. Chem. Phys.* **1985**, *82*, 552.
7. Dannhauser, T.; Johansson, K.; Whitten, D. Photophysics of Quantized Colloidal Semiconductors. Dramatic Luminescence Enhancement by Binding of Simple Amines. *J. Phys. Chem.* **1986**, *90*, 6074–6076.
8. Novoselov, K. S.; Jiang, D.; Schedin, F.; Booth, T. J.; Khotkevich, V. V.; Morozov, S. V.; Geim, A. K. Two-Dimensional Atomic Crystals. *Proc. Natl. Acad. Sci. U. S. A.* **2005**, *102*, 10451–10453.
9. Mak, K. F.; Lee, C.; Hone, J.; Shan, J.; Heinz, T. F. Atomically Thin MoS_2: A New Direct-Gap Semiconductor. *Phys. Rev. Lett.* **2010**, *105*, 136805.
10. Yun, W. S.; Han, S.; Hong, S. C.; Kim, I. G.; Lee, J. Thickness and Strain Effects on Electronic Structures of Transition Metal Dichalcogenides: 2H-MX_2 Semiconductors (M = Mo, W; X = S, Se, Te). *Phys. Rev. B: Condens. Matter Mater. Phys.* **2012**, *85*, 033305.
11. Gorer, S.; Albu-Yaron, A.; Hodes, G. Quantum Size Effects in Chemically Deposited, Nanocrystalline Lead Selenide Films. *J. Phys. Chem.* **1995**, *99*, 16442–16448.
12. Kang, I.; Wise, F. W. Electronic Structure and Optical Properties of PbS and PbSe Quantum Dots. *J. Opt. Soc. Am. B* **1997**, *14*, 1632.
13. Pietryga, J. M.; Schaller, R. D.; Werder, D.; Stewart, M. H.; Klimov, V. I.; Hollingsworth, J. A. Pushing the Band Gap Envelope: Mid-Infrared Emitting Colloidal PbSe Quantum Dots. *J. Am. Chem. Soc.* **2004**, *126*, 11752–11753.
14. Bridgman, P. W. Two New Modifications of Phosphorus. *J. Am. Chem. Soc.* **1914**, *36*, 1344–1363.
15. Li, L.; Yu, Y.; Ye, G. J.; Ge, Q.; Ou, X.; Wu, H.; Feng, D.; Chen, X. H.; Zhang, Y. Black Phosphorus Field-Effect Transistors. *Nat. Nanotechnol.* **2014**, *9*, 372–377.
16. Liu, H.; Neal, A. T.; Zhu, Z.; Luo, Z.; Xu, X.; Tománek, D.; Ye, P. D. Phosphorene: An Unexplored 2D Semiconductor with a High Hole Mobility. *ACS Nano* **2014**, *8*, 4033–4041.
17. Morita, A. Semiconducting Black Phosphorus. *Appl. Phys. A: Solids Surf.* **1986**, *39*, 227–242.
18. Li, L.; Yu, Y.; Ye, G. J.; Ge, Q.; Ou, X.; Wu, H.; Feng, D.; Chen, X. H.; Zhang, Y. Black Phosphorus Field-Effect Transistors. *Nat. Nanotechnol.* **2014**, *9*, 372–377.
19. Koenig, S. P.; Doganov, R. A.; Schmidt, H.; Castro Neto, A. H.; Özyilmaz, B. Electric Field Effect in Ultrathin Black Phosphorus. *Appl. Phys. Lett.* **2014**, *104*, 103106.
20. Buscema, M.; Groenendijk, D. J.; Steele, G. A.; van der Zant, H. S. J. Photovoltaic Effect in Few-Layer Black Phosphorus PN Junctions Defined by Local Electrostatic Gating. *Nat. Commun.* **2014**, *5*, 4651.
21. Deng, Y.; Luo, Z.; Conrad, N. J.; Liu, H.; Gong, Y.; Najmaei, S.; Ajayan, P. M.; Lou, J.; Xu, X.; Ye, P. D. Black Phosphorus-Monolayer MoS_2 van Der Waals Heterojunction P-N Diode. *ACS Nano* **2014**, *8*, 8292–8298.
22. Engel, M.; Steiner, M.; Avouris, P. A Black Phosphorus Photo-Detector for Multispectral, High-Resolution Imaging. *Nano Lett.* **2014**, *14*, 6414–6417.
23. Low, T.; Engel, M.; Steiner, M.; Avouris, P. Origin of Photoresponse in Black Phosphorus Phototransistors. *Phys. Rev. B: Condens. Matter Mater. Phys.* **2014**, *90*, 081408.
24. Park, C.-M.; Sohn, H.-J. Black Phosphorus and Its Composite for Lithium Rechargeable Batteries. *Adv. Mater.* **2007**, *19*, 2465–2468.
25. Cunningham, G.; Lotya, M.; Cucinotta, C. S.; Sanvito, S.; Bergin, S. D.; Menzel, R.; Shaffer, M. S. P.; Coleman, J. N. Solvent Exfoliation of Transition Metal Dichalcogenides: Dispersibility of Exfoliated Nanosheets Varies Only Weakly Between Compounds. *ACS Nano* **2012**, *6*, 3468–3480.
26. Fei, R.; Yang, L. Strain-Engineering the Anisotropic Electrical Conductance of Few-Layer Black Phosphorus. *Nano Lett.* **2014**, *14*, 2884–2889.
27. Low, T.; Rodin, A. S.; Carvalho, A.; Jiang, Y.; Wang, H.; Xia, F.; Neto, A. H. C. Tunable Optical Properties of Multilayers Black Phosphorus. *Phys. Rev. B* **2014**, *90*, 075434.
28. Castellanos-Gomez, A.; Vicarelli, L.; Prada, E.; Island, J. O.; Narasimha-Acharya, K. L.; Blanter, S. I.; Groenendijk, D. J.; Buscema, M.; Steele, G. A.; Alvarez, J. V.; et al. Isolation and Characterization of Few-Layer Black Phosphorus. *2D Mater.* **2014**, *1*, 025001.
29. Jiang, J.-W.; Park, H. S. Mechanical Properties of Single-Layer Black Phosphorus. *J. Phys. D: Appl. Phys.* **2014**, *47*, 385304.
30. Kou, L.; Frauenheim, T.; Chen, C. Phosphorene as a Superior Gas Sensor: Selective Adsorption and Distinct I - V Response. *J. Phys. Chem. Lett.* **2014**, *5*, 2675–2681.
31. Zhang, R.; Li, B.; Yang, J. First-Principles Study of the Interactions of Electron Donor and Acceptor Molecules with Phosphorene. *arXiv:1409.7190* **2014**.
32. Favron, A.; Gaufrès, E.; Fossard, F.; Phaneuf-L'Heureux, A.-L.; Tang, N. Y.-W.; Lévesque, P. L.; Loiseau, A.; Leonelli, R.; Francoeur, S.; Martel, R. Photooxidation and Quantum Confinement Effects in Exfoliated Black Phosphorus. *Nat. Mater.* **2015**, *14*, 826–832.
33. Ziletti, A.; Carvalho, A.; Campbell, D. K.; Coker, D. F.; Castro Neto, A. H. Oxygen Defects in Phosphorene. *Phys. Rev. Lett.* **2015**, *114*, 046801.
34. Carvalho, A.; Rodin, A. S.; Castro Neto, A. H. Phosphorene Nanoribbons. *Europhys. Lett.* **2014**, *108*, 47005.
35. Xie, J.; Si, M. S.; Yang, D. Z.; Zhang, Z. Y.; Xue, D. S. A Theoretical Study of Blue Phosphorene Nanoribbons Based on First-Principles Calculations. *J. Appl. Phys.* **2014**, *116*, 073704.
36. Guan, J.; Zhu, Z.; Tomanek, D. High Stability of Faceted Nanotubes and Fullerenes of Multi-Phase Layered Phosphorus: A Computational Study. *Phys. Rev. Lett.* **2014**, *113*, 226801.
37. Tran, V.; Soklaski, R.; Liang, Y.; Yang, L. Layer-Controlled Band Gap and Anisotropic Excitons in Few-Layer Black Phosphorus. *Phys. Rev. B: Condens. Matter Mater. Phys.* **2014**, *89*, 235319.
38. Xia, F.; Wang, H.; Jia, Y. Rediscovering Black Phosphorus as an Anisotropic Layered Material for Optoelectronics and Electronics. *Nat. Commun.* **2014**, *5*, 4458.
39. Buscema, M.; Groenendijk, D. J.; Blanter, S. I.; Steele, G. A.; van der Zant, H. S. J.; Castellanos-Gomez, A. Fast and Broadband Photoresponse of Few-Layer Black Phosphorus Field-Effect Transistors. *Nano Lett.* **2014**, *14*, 3347–3352.
40. Hernandez, Y.; Nicolosi, V.; Lotya, M.; Blighe, F. M.; Sun, Z.; De, S.; McGovern, I. T.; Holland, B.; Byrne, M.; Gun'Ko, Y. K.; et al. High-Yield Production of Graphene by Liquid-Phase Exfoliation of Graphite. *Nat. Nanotechnol.* **2008**, *3*, 563–568.
41. Coleman, J. N.; Lotya, M.; O'Neill, A.; Bergin, S. D.; King, P. J.; Khan, U.; Young, K.; Gaucher, A.; De, S.; Smith, R. J.; et al. Two-Dimensional Nanosheets Produced by Liquid Exfoliation of Layered Materials. *Science* **2011**, *331*, 568–571.
42. Warren, S. C.; Woomer, A. H.; Wells, R. A.; Farnsworth, T. W. Two Dimensional Materials Produced by the Liquid Exfoliation of Black Phosphorus. U.S. Patent appl. 62/031,184, **2014**.
43. Brent, J. R.; Savjani, N.; Lewis, E. A.; Haigh, S. J.; Lewis, D. J.; O'Brien, P. Production of Few-Layer Phosphorene by Liquid Exfoliation of Black Phosphorus. *Chem. Commun.* **2014**, *50*, 13338–13341.
44. Yasaei, P.; Kumar, B.; Foroozan, T.; Wang, C.; Asadi, M.; Tuschel, D.; Indacochea, J. E.; Klie, R. F.; Salehi-Khojin, A. High-Quality Black Phosphorus Atomic Layers by Liquid-Phase Exfoliation. *Adv. Mater.* **2015**, *27*, 1887–1892.
45. Kang, J.; Wood, J. D.; Wells, S. A.; Lee, J.-H.; Liu, X.; Chen, K.-S.; Hersam, M. C. Solvent Exfoliation of Electronic-Grade, Two-Dimensional Black Phosphorus. *ACS Nano* **2015**, *9*, 3596–3604.
46. Köpf, M.; Eckstein, N.; Pfister, D.; Grotz, C.; Krüger, I.; Greiwe, M.; Hansen, T.; Kohlmann, H.; Nilges, T. Access and *In Situ* Growth of Phosphorene-Precursor Black Phosphorus. *J. Cryst. Growth* **2014**, *405*, 6–10.
47. Stadelmann, P. *JEMS - EMS*, Java version; http://cimewww.epfl.ch/people/stadelmann/jemsWebSite/jems.html.
48. Ci, L.; Song, L.; Jin, C.; Jariwala, D.; Wu, D.; Li, Y.; Srivastava, A.; Wang, Z. F.; Storr, K.; Balicas, L.; et al. Atomic Layers of Hybridized Boron Nitride and Graphene Domains. *Nat. Mater.* **2010**, *9*, 430–435.

49. Gass, M. H.; Bangert, U.; Bleloch, A. L.; Wang, P.; Nair, R. R.; Geim, A. K. Free-Standing Graphene at Atomic Resolution. *Nat. Nanotechnol.* **2008**, *3*, 676–681.
50. Goodman, N. B.; Ley, L.; Bullett, D. W. Valence-Band Structures of Phosphorus Allotropes. *Phys. Rev. B: Condens. Matter Mater. Phys.* **1983**, *27*, 7440–7450.
51. Moulder, J. F.; Stickle, W. F.; Sobol, P. E.; Bomben, K. D. *Handbook of X-ray Photoelectron Spectroscopy*; Physical Electronics Division, Perkin-Elmer Corp: Eden Prairie, Minnesota, 1979; Vol. 3.
52. Wood, J. D.; Wells, S. A.; Jariwala, D.; Chen, K.-S.; Cho, E.; Sangwan, V. K.; Liu, X.; Lauhon, L. J.; Marks, T. J.; Hersam, M. C. Effective Passivation of Exfoliated Black Phosphorus Transistors against Ambient Degradation. *Nano Lett.* **2014**, *14*, 6964–6970.
53. Paton, K. R.; Varrla, E.; Backes, C.; Smith, R. J.; Khan, U.; O'Neill, A.; Boland, C.; Lotya, M.; Istrate, O. M.; King, P.; et al. Scalable Production of Large Quantities of Defect-Free Few-Layer Graphene by Shear Exfoliation in Liquids. *Nat. Mater.* **2014**, *13*, 624–630.
54. Paton, K. Personal communication.
55. Takao, Y.; Asahina, H.; Morita, A. Electronic Structure of Black Phosphorus in Tight Binding Approach. *J. Phys. Soc. Jpn.* **1981**, *50*, 3362–3369.
56. Klingshirn, C. *Semiconductor Optics*; Springer: Berlin, 2007.
57. Degoli, E.; Cantele, G.; Luppi, E.; Magri, R.; Ninno, D.; Bisi, O.; Ossicini, S. Ab Initio Structural and Electronic Properties of Hydrogenated Silicon Nanoclusters in the Ground and Excited State. *Phys. Rev. B: Condens. Matter Mater. Phys.* **2004**, *69*, 155411.
58. Choi, J. H.; Strano, M. S. Solvatochromism in Single-Walled Carbon Nanotubes. *Appl. Phys. Lett.* **2007**, *90*, 223114.
59. Jackson, W. B.; Kelso, S. M.; Tsai, C. C.; Allen, J. W.; Oh, S.-J. Energy Dependence of the Optical Matrix Element in Hydrogenated Amorphous and Crystalline Silicon. *Phys. Rev. B: Condens. Matter Mater. Phys.* **1985**, *31*, 5187–5198.
60. Mott, N. F. In *Electronic Processes in Non-Crystalline Materials*, 2nd ed.; Davis, E. A., Ed.; Clarendon Press: Oxford, U.K., 1979.
61. Yang, J.; Xu, R.; Pei, J.; Myint, Y. W.; Wang, F.; Wang, Z.; Yu, Z.; Lu, Y. Unambiguous Identification of Monolayer Phosphorene by Phase-Shifting Interferometry. *arXiv:1412.6701* **2014**.
62. Wang, X.; Jones, A. M.; Seyler, K. L.; Tran, V.; Jia, Y.; Wang, H.; Yang, L.; Xu, X.; Xia, F. Highly Anisotropic and Robust Excitons in Monolayer Black Phosphorus. *Nat. Nanotechnol.* **2015**, *10*, 517–521.
63. Zhang, S.; Yang, J.; Xu, R.; Wang, F. Extraordinary Photoluminescence and Strong Temperature/Angle-Dependent Raman Responses in Few-Layer Phosphorene. *ACS Nano* **2014**, *8*, 9590–9596.
64. Das, S.; Zhang, W.; Demarteau, M.; Hoffmann, A.; Dubey, M.; Roelofs, A. Tunable Transport Gap in Phosphorene. *Nano Lett.* **2014**, *14*, 5733–5739.
65. Liang, L.; Wang, J.; Lin, W.; Sumpter, B. G.; Meunier, V.; Pan, M. Electronic Bandgap and Edge Reconstruction in Phosphorene Materials. *Nano Lett.* **2014**, *14*, 6400–6406.
66. Rudenko, A. N.; Katsnelson, M. I. Quasiparticle Band Structure and Tight-Binding Model for Single- and Bilayer Black Phosphorus. *Phys. Rev. B: Condens. Matter Mater. Phys.* **2014**, *89*, 1–5.
67. Qiao, J.; Kong, X.; Hu, Z.-X.; Yang, F.; Ji, W. High-Mobility Transport Anisotropy and Linear Dichroism in Few-Layer Black Phosphorus. *Nat. Commun.* **2014**, *5*, 4475.
68. Elliott, R. Intensity of Optical Absorption by Excitons. *Phys. Rev.* **1957**, *108*, 1384–1389.
69. Wannier, G. The Structure of Electronic Excitation Levels in Insulating Crystals. *Phys. Rev.* **1937**, *52*, 191–197.
70. Tauc, J. Optical Properties and Electronic Structure of Amorphous Ge and Si. *Mater. Res. Bull.* **1968**, *3*, 37–46.
71. Baba, M.; Nakamura, Y.; Shibata, K.; Morita, A. Photoconduction of Black Phosphorus in the Infrared Region. *Jpn. J. Appl. Phys.* **1991**, *30*, L1178.
72. Keyes, R. The Electrical Properties of Black Phosphorus. *Phys. Rev.* **1953**, *92*, 580.
73. Warschauer, D. Electrical and Optical Properties of Crystalline Black Phosphorus. *J. Appl. Phys.* **1963**, *34*, 1853–1860.
74. Maruyama, Y.; Suzuki, S.; Kobayashi, K.; Tanuma, S. Synthesis and Some Properties of Black Phosphorus Single Crystals. *Physica B+C* **1981**, *105*, 99–102.
75. Shirotani, I. Growth of Large Single Crystals of Black Phosphorus at High Pressures and Temperatures, and Its Electrical Properties. *Mol. Cryst. Liq. Cryst.* **1982**, *86*, 203–211.
76. Akahama, Y.; Endo, S.; Narita, S. I. Electrical Properties of Black Phosphorus Single Crystals. *J. Phys. Soc. Jpn.* **1983**, *52*, 2148–2155.
77. Hecht, E.; Ganesan, A. R. *Optics*, 4th ed.; Dorling Kindersley: London, 2008.
78. Urbach, F. The Long-Wavelength Edge of Photographic Sensitivity and of the Electronic Absorption of Solids. *Phys. Rev.* **1953**, *92*, 1324.
79. Brus, L. E. Electron–Electron and Electron-Hole Interactions in Small Semiconductor Crystallites: The Size Dependence of the Lowest Excited Electronic State. *J. Chem. Phys.* **1984**, *80*, 4403.
80. Rudenko, A. N.; Katsnelson, M. I. Quasiparticle Band Structure and Tight-Binding Model for Single- and Bilayer Black Phosphorus. *Phys. Rev. B: Condens. Matter Mater. Phys.* **2014**, *89*, 201408.
81. Perebeinos, V.; Tersoff, J.; Avouris, P. Scaling of Excitons in Carbon Nanotubes. *Phys. Rev. Lett.* **2004**, *92*, 257402.
82. Wang, V.; Kawazoe, Y.; Geng, W. T. Native Point Defects in Few-Layer Phosphorene. *Phys. Rev. B: Condens. Matter Mater. Phys.* **2015**, *91*, 45433.
83. Yuan, H.; Liu, X.; Afshinmanesh, F.; Li, W.; Xu, G.; Sun, J.; Lian, B.; Ye, G.; Hikita, Y.; Shen, Z.; et al. Polarization-sensitive broadband photodetector using a black phosphorus vertical p–n junction. *Nat. Nanotechnol.* **2015**, *10*, 707.
84. Splendiani, A.; Sun, L.; Zhang, Y.; Li, T.; Kim, J.; Chim, C.-Y.; Galli, G.; Wang, F. Emerging Photoluminescence in Monolayer MoS_2. *Nano Lett.* **2010**, *10*, 1271–1275.
85. Murray, C. B.; Norris, D.; Bawendi, M. G. Synthesis and Characterization of Nearly Monodisperse CdE (E= S, Se, Te) Semiconductor Nanocrystallites. *J. Am. Chem. Soc.* **1993**, *115*, 8706–8715.